

# Metal-insulator transition and topological properties of pyrochlore iridates

Hongbin Zhang, Kristjan Haule, and David Vanderbilt  
*Department of Physics and Astronomy, Rutgers University, Piscataway, USA*  
 (Dated: April 8, 2015)

Combining density functional theory (DFT) and embedded dynamical mean-field theory (DMFT) methods, we study the metal-insulator transition in  $R_2\text{Ir}_2\text{O}_7$  ( $R=\text{Y, Eu, Sm, Nd, Pr, and Bi}$ ) and the topological nature of the insulating compounds. Accurate free energies evaluated using the charge self-consistent DFT+DMFT method reveal that the metal-insulator transition occurs for an A-cation radius between that of Nd and Pr, in agreement with experiments. The all-in-all-out magnetic phase, which is stable in the Nd compound but not the Pr one, gives rise to a small  $\text{Ir}^{4+}$  magnetic moment of  $\approx 0.5\mu_B$  and opens a sizable correlated gap. We demonstrate that within this state-of-the-art theoretical method, the insulating bulk pyrochlore iridates are topologically trivial.

Interest in  $5d$  compounds has blossomed in recent years, as they provide a promising playground for interesting new physics<sup>1–5</sup> arising from the interplay of the atomic spin-orbit coupling (SOC), which scales as  $Z^4$  with the atomic number  $Z$ , and the electronic correlations, which are reduced due to the spatially more extended wavefunctions of the  $5d$  ions. Rare-earth pyrochlore iridates ( $R_2\text{Ir}_2\text{O}_7$ ) have drawn intensive attention in recent years<sup>6</sup> because of their geometrically frustrated lattice, which favors the spin-liquid phase,<sup>7</sup> and the possibility to host various nontrivial topological phases in the bulk,<sup>8–12</sup> thin films,<sup>13,14</sup> and domain walls.<sup>15</sup> Depending on the radius of the A-site cation, rare-earth pyrochlore iridates undergo a metal-insulator transition (MIT),<sup>16</sup> concomitant with a transition to an all-in-all-out (AIAO) magnetic state.<sup>17–19</sup> Nevertheless, when the A-site cation is Pr or the more covalent Bi, the corresponding pyrochlore iridates are metallic down to very low temperature with no long-range magnetic ordering.<sup>7,20</sup>

Recently, inspired by pioneering work based on a generic tight-binding model,<sup>8</sup> there have been many studies focusing on nontrivial topological phases in bulk pyrochlore iridates.<sup>9–12</sup> Based on calculations using the local density approximation (LDA) with Hubbard  $U$  (LDA+ $U$ ) including SOC, Wan *et al.* predicted that  $\text{Y}_2\text{Ir}_2\text{O}_7$  can host nontrivial Weyl semimetal and axion insulator phases.<sup>11</sup> Using a simplified single-band Hubbard model on the pyrochlore lattice, Go *et al.* conducted cluster-DMFT calculations<sup>12</sup> and confirmed the LDA+ $U$ +SOC phase diagram, but with a magnetic configuration having the Ir magnetic moments rotated by  $90^\circ$  from the AIAO ground-state configuration.

Iridates are known to be beyond the range of applicability of LDA+ $U$  calculations, since dynamical local correlations are crucial to explain their complicated electronic structure. Instead, the LDA+DMFT method<sup>21</sup> correctly gives the boundary of the MIT in the Ruddlesden-Popper (RP) series, and the fine details of the ARPES measurements of  $\text{Sr}_2\text{IrO}_4$ <sup>22</sup> can only be understood by comparing with the LDA+DMFT spectral functions, which include essentially exact correlation effects local to a given Ir atom.<sup>21</sup> Moreover, the LDA+ $U$  method overestimates the stability of the insulating mag-

netically ordered states, and the value of  $U$ , which is to some extent an adjustable parameter, often needs to be adjusted for each member of the series. Thus, a consistent treatment of the electronic correlations together with spin-orbit coupling at the LDA+DMFT level is necessary to shed light on the MIT in the pyrochlore iridates.

In this work, we have carried out all-electron charge self-consistent LDA+DMFT<sup>23</sup> calculations. We have studied a series of pyrochlore iridates in both the paramagnetic (PM) and AIAO magnetic states, focusing on the metal-insulator transition with respect to the A-cation radius and the topological nature of the insulating states. We demonstrate that the MIT occurs in those compounds which can host an AIAO magnetic ground state. Because of the large degree of geometric frustration in the pyrochlore lattice, a significant quasiparticle mass in the PM state is needed to destabilize the Fermi liquid formation at the expense of magnetic long-range order. The tuning across the boundary between the Kondo-screened Fermi-liquid solution and the magnetic AIAO solution is achieved with A-cation substitution. The most important consequence of the latter is the change of oxygen coordinates, which results in a slightly different Ir hybridization and effective Ir- $t_{2g}$  bandwidth. Based on calculations of the wavefunction parities in a many-body context, we conclude that the insulating pyrochlore iridates are likely to remain topologically trivial.

Our LDA+DMFT calculations were done using the projection/embedding implementation,<sup>23</sup> which avoids downfolding or model building, and adds dynamic local correlations to a set of localized quasi-atomic orbitals. The DFT part is implemented using the WIEN2k package.<sup>24</sup> All parameters of the calculation are identical to those used in our earlier work on RP iridates.<sup>21</sup> We also performed LDA+ $U$  calculations using the VASP code<sup>25</sup> for comparison. Details are provided in the Supplemental Materials.

For the series of  $R_2\text{Ir}_2\text{O}_7$  ( $R=\text{Y, Eu, Sm, Nd, Pr, and Bi}$ ) compounds, we considered the PM and AIAO magnetic solutions. We found that the magnetic AIAO solution could be stabilized (that is, we could find a stable or metastable solution) only in the Y, Eu, Sm, and Nd compounds, and was always insulating (see spectral functions in the Supplement), while the PM solution could be

stabilized for all materials and was always metallic, consistent with experiments.<sup>16,20</sup> Naively, the MIT in the six  $R_2\text{Ir}_2\text{O}_7$  compounds can be understood in terms of the bandwidth of the Ir- $t_{2g}$  bands, as shown as inset of Fig. 1(a). For instance, at the LDA level there is a critical value of about 2.6 eV for the Ir- $t_{2g}$  bandwidth separating the compounds with insulating and metallic ground states. A detailed analysis reveals that the bandwidth is closely correlated with the hybridization function, and its variation can be attributed to the change of the oxygen coordinates (see the Supplement).

To determine the relative stability of the two phases, we computed the free energy differences between PM and AIAO states following Ref. 26, yielding the results displayed in Fig. 1(a). For comparison, the difference of LDA+U total energies is also shown, but reduced by a factor of 20 to fit in the plot. For each method, we used the same  $U$  as determined in our previous study of RP iridates.<sup>21</sup> The LDA+U energy difference is about 400 meV on average, much too large to be compatible with the known ordering temperatures. This is hardly surprising since the local moments are zero in the PM state within LDA+U, which cannot describe fluctuating local moments. As a result, the energy of the PM state is severely overestimated.

Experimentally,  $\text{Pr}_2\text{Ir}_2\text{O}_7$  has a non-magnetic metallic ground state,<sup>16</sup> correctly described by LDA+DMFT. In LDA+U by contrast, only  $\text{Bi}_2\text{Ir}_2\text{O}_7$  is metallic, while the ground state of  $\text{Pr}_2\text{Ir}_2\text{O}_7$  is an AIAO magnetic insulator. We also studied other possible magnetic phases within LDA+DMFT. We found that the three-in-one-out configuration can also be stabilized for some compounds, but is higher in energy than the AIAO state (*e.g.*, by 23 meV for  $\text{Y}_2\text{Ir}_2\text{O}_7$ ). The two-in-two-out state, on the other hand, is not stable in this method. Therefore, the AIAO magnetic state is indeed the ground state of insulating pyrochlore iridates within LDA+DMFT.

Our self-consistent LDA+DMFT calculations also give reasonable estimates of the free-energy differences between PM and AIAO states as shown in Fig. 1(a). The average free-energy difference is about 20 meV, which is about twice the typical magnetic ordering temperature (about 100 K) observed experimentally.<sup>16</sup> Moreover, the trend of the LDA+DMFT free-energy difference with respect to the A-cation radius follows loosely the experimental magnetic ordering temperature.<sup>16,20</sup> We note in passing that the difference in electronic entropy  $S$  between the two phases is very small. For example, in  $\text{Nd}_2\text{Ir}_2\text{O}_7$  we obtained  $\Delta S = 0.033 k_B$  per Ir atom, which is similar to the experimentally determined  $\Delta S = 0.028 k_B$ <sup>16</sup> (see the Supplement).

To shed more light on the origin of the MIT, Fig. 1(b) shows the DMFT-predicted quasiparticle renormalization amplitude  $Z_\alpha = (1 - d\text{Im}\Sigma_{\alpha\alpha}/d\omega_n)^{-1}|_{\omega_n=0}$ , where  $\alpha$  labels a correlated orbital and  $\Sigma$  indicates the self-energy on the Matsubara-frequency ( $\omega_n$ ) axis. The less active  $J_{\text{eff}} = 3/2$  states are only weakly renormalized. Turning to the more active  $J_{\text{eff}} = 1/2$  states, these are

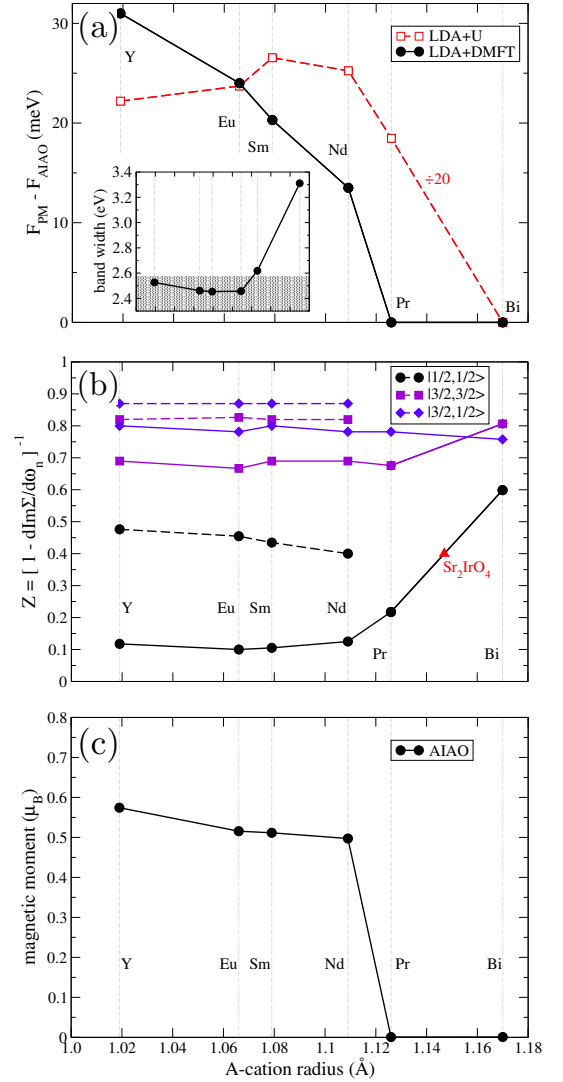


FIG. 1: (Color online) Variation with respect to the A-cation radius of computed properties of  $R_2\text{Ir}_2\text{O}_7$  ( $R = \text{Y, Eu, Sm, Nd, Pr, Bi}$ ). (a) Difference of free energies  $F$  between PM and AIAO magnetic states for  $R_2\text{Ir}_2\text{O}_7$ . Solid circles (hollow squares) denote the values obtained using the LDA+DMFT (LDA+U) method, plotted as zero when the AIAO state cannot be stabilized. Inset displays the LDA band-width of the  $t_{2g}$  bands; shaded region highlights the insulating compounds. (b) Quasiparticle renormalization amplitude  $Z_\alpha$  (see text for the definition) for the  $J_{\text{eff}} = 1/2$  and  $J_{\text{eff}} = 3/2$  states. Solid (dashed) lines denote the values in the PM (AIAO) states, with  $Z$  for the  $J_{\text{eff}} = 1/2$  orbital in the PM state of  $\text{Sr}_2\text{IrO}_4$  (red triangle) shown for comparison. (c) Ordered moment of Ir atoms. All LDA+DMFT calculations are done at 50 K.

renormalized by a factor of almost ten in the PM state for compounds having an insulating ground state. By contrast, the  $J_{\text{eff}} = 1/2$  quasiparticles in  $\text{Bi}_2\text{Ir}_2\text{O}_7$  remain quite light, consistent with recent ARPES measurement.<sup>27</sup> Surprisingly, the  $J_{\text{eff}} = 1/2$  orbital in  $\text{Pr}_2\text{Ir}_2\text{O}_7$  is quite heavy (about five times the band mass), indicating that the correlations are considerably stronger than in

the marginal Mott insulator  $\text{Sr}_2\text{IrO}_4$ , whose  $Z_\alpha$  is plotted as the red triangle in Fig. 1(b). In this sense, the frustration in the pyrochlore lattice plays an essential role in shifting the MIT boundary towards stronger correlations compared to unfrustrated RP iridates. The frustration thus promotes metallicity by penalizing competing long-range magnetic order, an effect which is well captured by DMFT but less adequately by LDA+U, explaining why LDA+U predicts the Pr compound to be insulating.

In short, the boundary of the MIT across the  $R_2\text{Ir}_2\text{O}_7$  compounds is determined by a competition between the formation of a quasiparticle band via the Kondo effect in the PM state, and the tendency toward long-range magnetic order. Both can lead to an effective reduction of the free energy, and are favored by enhanced quantum fluctuations. In general, the occurrence of a MIT depends crucially on many factors, including dimensionality and frustration. For example, in  $\text{Sr}_2\text{IrO}_4$  the two-dimensionality reduces the Néel ordering temperature, but the short-range order above the Néel temperature still preserves the charge gap in the excitation spectrum. Frustration also reduces the tendency to long-range order, but it promotes metallicity and allows very narrow quasiparticles to be observed in the PM state before the long-range order opens the charge gap. This is why  $\text{Pr}_2\text{Ir}_2\text{O}_7$  remains in the paramagnetic bad-metal phase even though the correlation strength is much larger than in  $\text{Sr}_2\text{IrO}_4$ .

For correlated Fermi liquids, the quantum fluctuations give rise to fluctuating moments in the PM state, which statically order when the magnetic energy gain is sufficient to overcome the gain available from band formation. According to Fig. 1(c), the magnitude of the ordered magnetic moment for  $\text{Y}_2\text{Ir}_2\text{O}_7$  is about  $0.57 \mu_B$ . This is a bit larger than the experimental upper bound of  $0.5 \mu_B$  obtained by neutron scattering,<sup>18</sup> which can be attributed to the fact that the spatial fluctuations, which are not fully accounted for in LDA+DMFT, are likely to further reduce the ordered magnetic moment. In the AIAO insulating state, there are no states at the Fermi energy, but the slope of the self-energy at zero frequency still gives some measure of the importance of quantum fluctuations. As shown by the dashed lines in Fig. 1(b), the quantum renormalization effects are greatly reduced in the AIAO state as compared to the PM state.

We observed that, like the effective  $J_{\text{eff}} = 1/2$  states in the RP iridates,<sup>21</sup> the  $J_{\text{eff}} = 1/2$  wavefunction in the pyrochlore iridates also strongly deviates from the rotationally invariant  $\text{SU}(2)$  point. This is mostly due to the trigonal crystal field induced by compression of the  $\text{IrO}_6$  octahedra. The trigonal crystal-field splitting in our calculations is derived from a very large energy window, and is on average about 0.39 eV (see the Supplement), in good agreement with resonant X-ray scattering measurements.<sup>29</sup> Correspondingly, the resulting orbital-to-spin moment ratio is about 1.3 (see the Supplement), showing a significant deviation from the  $\text{SU}(2)$  limit of two.<sup>21</sup> Nevertheless, the effective  $J_{\text{eff}} = 1/2$  and  $J_{\text{eff}} = 3/2$  bands are still well separated in energy, which facili-

TABLE I: Parity analysis of eight eigenstates around  $E_F$  in the PM and AIAO magnetic states, corresponding to Figs. 2(a-b) respectively. ‘MULT’ denotes the multiplicity in accounting for the eight time-reversal invariant momenta. The parities are given in order of increasing energy eigenvalues, with vertical bars indicating  $E_F$ .

|          | MULT | PM                  | AIAO                |
|----------|------|---------------------|---------------------|
| $\Gamma$ | 1    | {+ + + +   + + + +} | {+ + + +   + + + +} |
| $L$      | 3    | {- - + +   + + + +} | {- + + +   - + + +} |
| $L'$     | 1    | {+ + - -   - - - -} | {+ - - -   + - - -} |
| $X$      | 3    | {+ + - -   + + - -} | {+ + - -   + + - -} |

tates our analysis of the topological character. Note that the values of local  $U$  and  $J$  parameters on Ir atoms in our LDA+DMFT calculations are the same for the pyrochlore and RP iridates,<sup>21</sup> confirming the more universal nature of local Coulomb repulsion across similar materials when the screening by hybridization effects at high energy are allowed in the calculation.

We now turn to the topological properties of the insulating pyrochlores. Fig. 2(a) shows a fictitious non-magnetic band structure of  $\text{Nd}_2\text{Ir}_2\text{O}_7$ , together with the irreducible representations for the  $J_{\text{eff}} = 1/2$  states around  $E_F$  at the eight time-reversal-invariant momenta (TRIM). This band structure is obtained by neglecting the dynamic part of the LDA+DMFT self-energy, but using the self-consistent LDA+DMFT charge density, with time-reversal (TR) symmetry imposed. We note that these bands are quite similar to the LDA bands.

Regarding the irreducible representations, the space group of the pyrochlore iridates is nonsymmorphic. Thus, depending on the choice of inversion center, the four energetically equivalent  $L$  points are separated into one  $L'$  and three  $L$  points, with opposite parities for the  $L'$  and  $L$  points as shown in Fig. 2(a). Moreover, at each of the three X points all states are four-fold degenerate by symmetry, with each degenerate group comprising two even-parity and two odd-parity states. Finally, all eight  $J_{\text{eff}} = 1/2$  bands at the  $\Gamma$  point have even parity. The situation is summarized in the PM column of Table I. It follows that if a global band gap could be opened so as to extend the shaded region of Fig. 2(a) throughout the Brillouin zone, corresponding to a half-filled  $J_{\text{eff}} = 1/2$  manifold, seven out of 16 of the occupied Kramers pairs at the eight TRIM would be odd-parity ones. Since this number is odd, it would generate a strong-topological-insulator phase.<sup>30</sup> It has been suggested this might be achieved for  $\text{Pr}_2\text{Ir}_2\text{O}_7$ , for example, by applying a strain along the (111) direction.<sup>31</sup> If the TR symmetry would be weakly broken in this phase, the system would become an axion rather than a strong topological insulator, but we shall use the term “topological insulator” to cover both cases.

When the DMFT self-energy is taken into account, the TR symmetry is spontaneously broken and a global gap opens up. However, the topological character may be different from that described above, because of the drastic

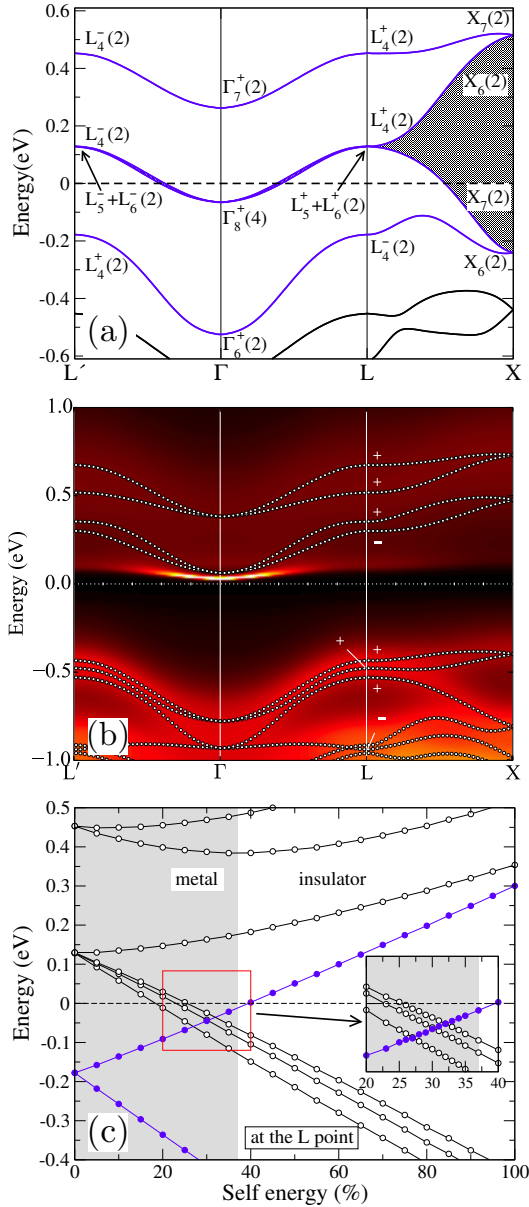


FIG. 2: (Color online) (a) The LDA-like band structure of  $\text{Nd}_2\text{Ir}_2\text{O}_7$  with irreducible representations indicated at the time-reversal invariant momenta; numbers in parenthesis denote degeneracies. (b) Color map: spectral function of  $\text{Nd}_2\text{Ir}_2\text{O}_7$  in the AIAO magnetic state. Dotted lines: band structure of the effective topological Hamiltonian (see text for details). The parities of eight  $J_{\text{eff}}=1/2$ -derived bands are indicated by “+” or “-” at the  $L$  point. (c) Evolution of the eigenvalues of the effective topological Hamiltonian at  $L$  with mixing fraction of the DMFT self-energy. Inset zooms in on the critical region indicated by the red square.

mixing of bands that results. Following the theory of interacting topological phases,<sup>32,33</sup> the topological indices can be obtained by inspecting an effective single-particle Hamiltonian defined as  $H_{\text{eff}}=H_0+\Sigma(\omega=0)$ , where  $H_0$  is the TR-invariant Bloch Hamiltonian and  $\Sigma(\omega=0)$  is the DMFT self-energy at zero frequency (i.e., at the Fermi

energy), which carries all the TR-breaking terms. The resulting band structure is shown in Fig. 2(b), together with the full LDA+DMFT spectral function. Since TR symmetry is broken, the total parity of all occupied eigenstates at the TRIM should now be counted;<sup>33</sup> the system will be a trivial or axion insulator if the total number is  $4n$  or  $4n+2$  respectively, with  $n$  an integer.

The parities of the  $J_{\text{eff}}=1/2$ -derived eigenstates at the eight TRIM are also shown for the AIAO state in Table I. At the  $\Gamma$  point all states remain even-parity even with the addition of the self-energy. At the  $X$  points, each four-fold degenerate state splits into two doublets, and we find (see the Supplement) that including  $\Sigma(\omega=0)$  does not induce any band inversion or otherwise change the ordering of parities, so that the number of occupied odd-parity states remains equal to two at each  $X$  point. The most significant change occurs at the  $L$  ( $L'$ ) points, where the TR-symmetry breaking splits each doubly-degenerate  $L_4^-$  ( $L_4^+$ ) state into two singlets. Some of these cross the gap as the self-energy is turned on, as shown in Fig. 2(c), with the result that there is an exchange of parity between occupied and unoccupied states as shown in Table I. As a result, there are a total of twelve odd-parity occupied states at the TRIM. Similar behavior is also observed in the other insulating  $R_2\text{Ir}_2\text{O}_7$  compounds studied. Thus, after properly including the DMFT self-energy, we find that the insulating  $R_2\text{Ir}_2\text{O}_7$  compounds are topologically trivial insulators. This is in agreement with previous LDA+U results<sup>11</sup> in the large- $U$  limit.

Nevertheless, in Refs. 11 and 12 it was argued that non-trivial axion insulator and Weyl semimetal phases occur with smaller values of on-site  $U$ . This is not supported by our DMFT calculations. For instance, for  $\text{Y}_2\text{Ir}_2\text{O}_7$ , which is the most insulating of the six compounds, the PM solution is more stable than the AIAO magnetic state when the on-site  $U$  value is reduced to 4.0 eV (see the Supplement). Moreover, as shown in Fig. 2(c), we observe that the parity exchange between occupied and unoccupied states at the  $L$  and  $L'$  points happens before a global band gap is opened. Therefore, we think it is very unlikely that a topological insulating phase can be found in the bulk pyrochlore iridates.

In summary, our calculations provide a clear picture of the origin of the MIT in pyrochlore iridates and its variation with respect to the A-cation radius. Moreover, our parity analysis of the many-body effective  $J_{\text{eff}}=1/2$  wave functions reveals that when insulating magnetic phases appear in these pyrochlore iridates, they are very likely to remain topologically trivial.

### Acknowledgments

We acknowledge Gregory A. Fiete, Victor Chua, Ru Chen, S.M. Disseler, Xiang Hu, Zhicheng Zhong, Jinjian Zhou, Yugui Yao, Jianpeng Liu, and Klaus Koepernik for helpful discussions. This work was supported by NSF Grant DMREF-12-33349.



Note: As we were finalizing this manuscript a preprint appeared<sup>34</sup> which presents results for  $\text{Y}_2\text{Ir}_2\text{O}_7$  that are similar to our own in some respects. However, we do

not agree that the magnetic moments on the Ir atoms in  $\text{Y}_2\text{Ir}_2\text{O}_7$  can be larger than  $1.0 \mu_B$  (see the Supplement for a detailed discussion).

- 
- <sup>1</sup> B.J. Kim, H. Jin, S.J. Moon, J.-Y. Kim, B.-G. Park, C.S. Leem, J. Yu, T.W. Noh, C. Kim, S.-J. Oh, J.-H. Park, V. Durairaj, G. Cao, and E. Rotenberg, *Phys. Rev. Lett.* **101**, 076402 (2008).
  - <sup>2</sup> B.J. Kim, H. Ohsumi, T. Komesu, S. Sakai, T. Morita, H. Takagi, and T. Arima, *Science* **323**, 1329 (2009).
  - <sup>3</sup> G. Jackeli and G. Khaliullin, *Phys. Rev. Lett.* **102**, 017205 (2009).
  - <sup>4</sup> A. Shitade, H. Katsura, J. Kuneš, X.-L. Qi, S.-C. Zhang, and N. Nagaosa, *Phys. Rev. Lett.* **102**, 256403 (2009).
  - <sup>5</sup> F. Wang and T. Senthil, *Phys. Rev. Lett.* **106**, 136402 (2011).
  - <sup>6</sup> W. Witczak-Krempa, G. Chen, Y.B. Kim, and L. Balents, *Ann. Rev. Condens. Matter Phys.* **5**, 57 (2014).
  - <sup>7</sup> See, for instance, Y. Tokiwa, J.J. Ishikawa, S. Nakatsuji, and P. Gegenwart, *Nat. Mat.* **13**, 356 (2014).
  - <sup>8</sup> D. Pesin, and L. Balents, *Nat. Phys.* **6**, 376 (2010).
  - <sup>9</sup> B.-J. Yang and Y.B. Kim, *Phys. Rev. B* **82**, 085111 (2010).
  - <sup>10</sup> M. Kargarian, J. Wen, and G.A. Fiete, *Phys. Rev. B* **83**, 165112 (2011).
  - <sup>11</sup> X. Wan, A.M. Turner, A. Vishwanath, and S.Y. Savrasov, *Phys. Rev. B* **83**, 205101 (2011).
  - <sup>12</sup> A. Go, W. Witczak-Krempa, G.S. Jeon, K. Park, and Y.B. Kim, *Phys. Rev. Lett.* **109**, 066401 (2012).
  - <sup>13</sup> X. Hu, A. Rüegg, and G.A. Fiete, *Phys. Rev. B* **86**, 235141 (2012); X. Hu, Z. Zhong, and G.A. Fiete, arXiv:1411.7333 (2014).
  - <sup>14</sup> B.-J. Yang and N. Nagaosa, *Phys. Rev. Lett.* **112**, 246402 (2014).
  - <sup>15</sup> Y. Yamaji and M. Imada, *Phys. Rev. X* **4**, 021035 (2014).
  - <sup>16</sup> K. Matsuhira, M. Wakeshima, Y. Hinatsu, and S. Takagi, *J. Phys. Soc. Jpn.* **80**, 094701 (2011).
  - <sup>17</sup> S.M. Disseler, C. Dhital, A. Amato, S.R. Giblin, C. de la Cruz, S.D. Wilson, and M.J. Graf, *Phys. Rev. B* **86**, 014428 (2012).
  - <sup>18</sup> M.C. Shapiro, S.C. Riggs, M.B. Stone, C.R. de la Cruz, S. Chi, A.A. Podlesnyak, and I.R. Fisher, *Phys. Rev. B* **85**, 214434 (2012).
  - <sup>19</sup> K. Tomiyasu, K. Matsuhira, K. Iwasa, M. Watahiki, S. Takagi, M. Wakeshima, Y. Hinatsu, M. Yokoyama, K. Ohoyama, and K. Yamada, *J. Phys. Soc. Jpn.* **81**, 034709 (2012).
  - <sup>20</sup> T.F. Qi, O.B. Korneta, X. Wan, L.E. DeLong, P. Schlottmann, and G. Cao, *J. Phys.: Condens. Matter* **24**, 345601 (2012).
  - <sup>21</sup> H. Zhang, K. Haule, and D. Vanderbilt, *Phys. Rev. Lett.* **111**, 246402 (2013).
  - <sup>22</sup> Q. Wang, Y. Cao, J.A. Waugh, S.R. Park, T.F. Qi, O.B. Korneta, G. Cao, and D.S. Dessau, *Phys. Rev. B* **87**, 245109 (2013).
  - <sup>23</sup> K. Haule, C.-H. Yee, and K. Kim, *Phys. Rev. B* **81**, 195107 (2010).
  - <sup>24</sup> <http://www.wien2k.at>
  - <sup>25</sup> <http://www.vasp.at>
  - <sup>26</sup> K. Haule, and T. Birol, arXiv:1501.06936.
  - <sup>27</sup> Q. Wang, Y. Cao, X.G. Wan, J.D. Denlinger, T.F. Qi, O.B. Korneta, G. Cao, and D.S. Dessau, *J. Phys.: Condens. Matter* **27**, 015502 (2015).
  - <sup>28</sup> Z.P. Yin, K. Haule, and G. Kotliar, *Nat. Mat.* **10**, 932 (2011).
  - <sup>29</sup> L. Hozoi, H. Gretarsson, J.P. Clancy, B.-G. Jeon, B. Lee, K.H. Kim, V. Yushankhai, P. Fulde, D. Casa, T. Gog, J. Kim, A.H. Said, M.H. Upton, Y.-J. Kim, J. van den Brink, *Phys. Rev. B* **89**, 115111 (2014).
  - <sup>30</sup> L. Fu, and C.L. Kane, *Phys. Rev. B* **76**, 045302 (2007).
  - <sup>31</sup> R. Chen, and L. Balents, *unpublished*.
  - <sup>32</sup> Z. Wang, and S.-C. Zhang, *Phys. Rev. X* **2**, 031008 (2012).
  - <sup>33</sup> A.M. Turner, Y. Zhang, R.S.K. Mong, and A. Vishwanath, *Phys. Rev. B* **85**, 165120 (2012).
  - <sup>34</sup> H. Shinaoka, S. Hoshino, M. Troyer, P. Werner, arXiv:1504.03962 (2015).